LA-UR-21-22189
Approved for public release; distribution is unlimited.

Title: The Impala's horn applied to posterior samples of Ti-6Al-4V strength model parameters

Author(s): Biswas, Ayan
Francom, Devin Craig
Luscher, Darby Jon
Plohr, JeeYeon Nam
Walters, David J.
Sjue, Sky K.

Intended for: Report

Issued: 2021-03-04

The Impala's horn applied to posterior samples of Ti-6Al-4V strength model parameters

Sky Sjue, Ayan Biswas, Devin Francom, D. J. Luscher,
JeeYeon Plohr and David Walters

1 Introduction

We have generated strength model parameters for the Preston-Tonks-Wallace (PTW) model of plastic deformation based on a collection of Ti-6Al-4V alloy data and a Bayesian framework [1]. This data collected from the literature includes different chemistries and processes. The experiments include quasistatic compression, Split Hopkinson Pressure Bar (SHPB) compression, and Taylor cylinders [2, 3, 4, 5, 6, 7, 8, 9, 10]. Here we use posterior parameter distributions applied to a hypothetical impact referred to as the Impala's horn. The Impala's horn is like a Taylor cylinder, but modified to have a conical profile that is truncated before coming to a point. The smaller diameter at the impact end results in higher calculated strain rates and strains than the same velocity impact with the traditional Taylor profile. The modified geometry exercises the behavior of the strength model outside the range of conditions found in the calibration data.

Here we sort posterior strength models based on their flow stress at characteristic values for this hypothetical deformation. Then we compare the performance of these posterior models based on two simple observable final state properties of the Impala's horn.

2 Geometry

The Impala's horn geometry used here has a maximum radius of 0.5 cm and a minimum radius of 0.15 cm, with a linear taper over length 5 cm. The Taylor cylinder simulation for comparison uses a constant radius of 0.5 cm over length 5 cm. For the results presented here, both are given an initial velocity of 180 m/s into a collision with a rigid flat surface. These geometries are shown in Figure 1.

Table 1: Comparison between characteristic quantities for the Impala horn and Taylor cylinder

quantity	Impala	Taylor
$\langle T \rangle$	694 K	359 K
$\langle \varepsilon \rangle$	0.6	0.06
$\langle \dot{\varepsilon} \rangle$	40,000/s	12,000/s

3 Effective values for posterior strength model samples

In order to sample the posterior distributions of the strength model parameters, we focus on quantities of interest for the Impala horn problem. We run a simulation in FLAG [11] with a nominal PTW strength model from our calibration, then find effective values of the temperature, strain and strain rate by tabulating the following quantities over the history of the simulation.

$$\langle \dot{\varepsilon} \rangle = \frac{1}{N_1} \int d\varepsilon \int d^3 r \dot{\varepsilon}(\varepsilon, \vec{r}) \tag{1}$$

$$\langle T \rangle = \frac{1}{N_1} \int d\varepsilon \int d^3 r T(\varepsilon, \vec{r}) \tag{2}$$

$$\langle \varepsilon \rangle = \frac{1}{N_2} \int d\varepsilon \int d^3 r \tag{3}$$

$$N_1 = \int d\varepsilon \int d^3 r \tag{4}$$

$$N_2 = \int_{\varepsilon_f > 0} d^3 r \tag{5}$$

The final quantities $\langle \varepsilon \rangle$, $\langle \dot{\varepsilon} \rangle$ and $\langle T \rangle$ are the effective values of the plastic strain, plastic strain rate and temperature for the deformation process in consideration. N_2 is simply the volume of the specimen being deformed. The integral over strain ensures that undeformed volumes do not distort the quantities of interest. One could similarly find values for the pressure ($\langle P \rangle$) or density ($\langle \rho \rangle$).

For an initial comparison, we run both the Taylor cylinder and the Impala horn to find the values in Table 1.

4 Summary

We compare the final length of the Impala's horn and the final radius of the deformed boot-like part at the impact end. These values are shown in Figure 2. These models resulting from the posterior ranking by flow stress are not unique when it comes to strain hardening and strain rate behavior, as shown in Figure 3. While we observe that the posterior parameters and the resulting strength

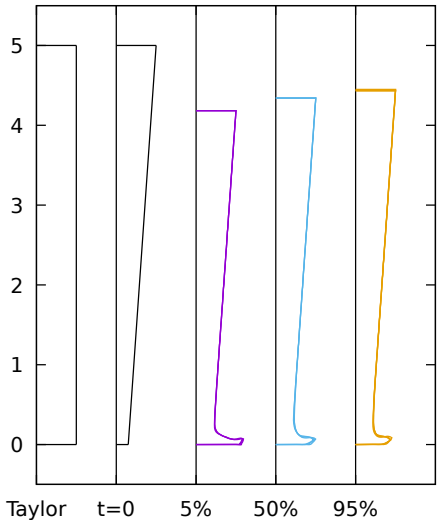

Figure 1: On the left is the profile of one half of a cylindrical sample with the traditional aspect ratio of a Taylor cylinder. At $t = 0$ is the pre-deformation profile of the Impala horn, with a conical shape tapering from $r = 0.5$ cm to $r = 0.15$ cm. The profiles labelled 5%, 50% and 95% show posterior samples sorted into percentiles based on the flow stress at the characteristic quantities given in Table 1. There are four profiles at 5% and 95% and three profiles at 50%.

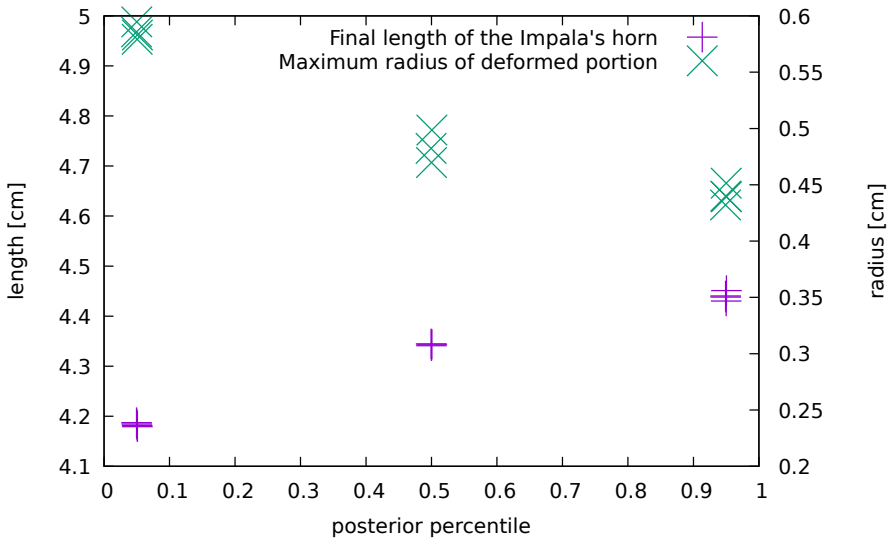

Figure 2: Comparison of the final length and maximum deformed radius of the Impala horn as a function of flow stress at the characteristic conditions. We also note that the nominal parameter values that were used to begin give results consistent with the 50% posterior samples, with a final length of 4.33 cm and a maximum final radius of 5.0 mm.

models differ significantly, they give very similar results for the Impala horn when ranked by flow stress at the effective values $\langle\varepsilon\rangle$, $\langle\dot{\varepsilon}\rangle$ and $\langle T\rangle$. Parameters for the eleven models selected from the posterior for this exercise are given in Table 2.

References

[1] Sky Sjue, James Ahrens, Ayan Biswas, Devin Francom, Earl Lawrence, Darby Luscher and David Walters, *"Fast strength model characterization using Bayesian statistics"* AIP Conference Proceedings **2272**, 070043 (2020).

[2] Frank J. Zerilli and Ronald W. Armstrong, *"Constitutive relations for titanium and Ti-6Al-4V,"* AIP Conference Proceedings **370**, 315 (1996).

[3] Woei-Shyan Lee and Chi-Feng Lin, *"Plastic deformation and fracture behaviour of Ti-6Al-4V alloy loaded with high strain rate under various temperatures,"* Materials Science and Engineering **A241**, 48–59 (1998).

[4] Sia Nemat-Nasser, Wei-Guo Guo, Vitali F. Nesterenko, S.S. Indrakanti and Ya-Bei Gu, *"Dynamic response of conventional and hot isostatically pressed*

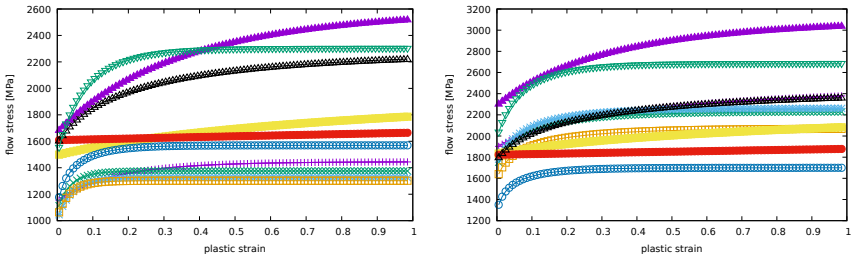

Figure 3: Comparisons of all posterior PTW models at strain rates of 2000/s (left) and 10^8/s (right) assuming isothermal behavior at T=300 K. Note that the relative behavior of these strength models varies widely from low to high rate.

Table 2: Posterior samples rated by flow stress at $\langle\varepsilon\rangle$, $\langle\dot{\varepsilon}\rangle$ and $\langle T\rangle$. The first row gives the nominal parameter set used to find the characteristic values in Table 1 to rank the posterior samples. The first column gives the sample's percentile from 2000 total posterior samples. The remaining parameters are part of the PTW model.

%	θ	p	s_0	s_∞	κ	γ	y_0	y_∞	y_1	y_2
nom	0.0375	1.00	0.0245	0.009	0.190	2.00e-6	0.0190	0.0076	0.0245	0.33
4.95	0.0264	2.67	0.0336	0.00628	0.305	7.77e-5	0.0256	0.00574	0.0613	0.611
5.00	0.123	2.77	0.0294	0.0046	0.269	4.31e-5	0.0225	0.00393	0.0656	0.669
5.05	0.110	1.97	0.0294	0.00714	0.339	2.64e-5	0.0221	0.00556	0.0606	0.834
5.10	0.126	3.01	0.0270	0.00601	0.287	3.32e-5	0.0208	0.005	0.0634	0.659
49.95	0.0081	3.55	0.0303	0.0104	0.128	4.76e-5	0.0235	0.0043	0.0676	0.576
50.00	0.183	2.37	0.0214	0.00912	0.0768	2.5e-5	0.0151	0.00705	0.0619	0.785
50.05	0.00076	2.27	0.0331	0.0217	0.0924	4.99e-5	0.0232	0.00633	0.0686	0.742
94.90	0.059	2.84	0.0307	0.0193	0.101	5.37e-5	0.0226	0.0086	0.0564	0.746
94.95	0.035	0.85	0.0396	0.0213	0.209	3.63e-5	0.0296	0.0072	0.0714	0.973
95.00	0.149	1.30	0.0340	0.0176	0.173	2.79e-5	0.0231	0.0093	0.0630	0.843
95.05	0.0035	4.19	0.0413	0.0286	0.0139	2.65e-5	0.0248	0.0051	0.0813	0.843

Ti-6Al-4V alloys: experiments and modeling," Mechanics of Materials **33**, 425–439 (2001).

[5] Akhtar S. Khan, Yeong Sung Suh and Rehan Kazmi, *"Quasi-static and dynamic loading responses and constitutive modeling of titanium alloys,"* International Journal of Plasticity **20**, 2233–2248 (2004).

[6] Songwoon Seo, Oakkey Min and Hyunmo Yang, *"Constitutive equation for Ti-6Al-4V at high temperature measured using the SHPB technique,"* International Journal of Impact Engineering **31**, 735–754 (2005).

[7] Akhtar S. Khan, Rehan Kazmi, Babak Farrokh and Marc Zupan, *"Effect of oxygen content and microstructure on thermo-mechanical response of three Ti-6Al-4V alloys: Experiments and modeling over a wide range of strain-rates and temperatures,"* International Journal of Plasticity **23**, 1105–1125 (2007).

[8] REN Yu, TAN Cheng-wen, ZHANG Jing and WANG Fu-chi, *"Dynamic fracture of Ti-6Al-4V alloy in Taylor impact test,"* Trans. Nonferrous Met. Soc. China **21**, 223–235 (2011).

[9] Guang Chen, Chengzu Ren, Xuda Qin and Jun Li, *"Temperature dependent work hardening in Ti-6Al-4V alloy over large temperature and strain ranges: Experiments and constitutive modeling,"* Materials & Design **83**, 598–610 (2015).

[10] A. Tabei, F.H. Abed, G.Z. Voyiadjis and H. Garmestani, *"Constitutive modeling of Ti-6Al-4V at a wide range of temperatures and strain rates,"* European Journal of Mechanics A/Solids **63**, 128–135 (2017).

[11] Donald E. Burton, *"Lagrangian Hydrodynamics in the FLAG Code,"* Advanced Numerical Methods for Lagrangian Hydrodynamics/LANL Report LA-UR-07-7547 (2007).